

1 **Discovery of Deccan Inclination Anomaly and its**
2 **possible geodynamic implications over the Indian**
3 **Plate**

4
5
6 **S. J. Sangode*, Ashish Dongre, Amarjeet Bhagat and Dhananjay Meshram**

7 *All affiliated to*

8 *Department of Geology, Savitribai Phule Pune University,*

9 *Pune (India) 411 007.*

10
11
12
13
14
15
16
17
18
19 **Corresponding author: sangode@rediffmail.com; sangode@unipune.ac.in*

20 *This paper is a non-peer reviewed preprint submitted to EarthArXiv.*

24 **Discovery of Deccan Inclination Anomaly and its**
25 **possible geodynamic implications over the Indian**
26 **Plate**

27 **S. J. Sangode*, Ashish Dongre, Amarjeet Bhagat and Dhananjay Meshram**

28 *Department of Geology, Savitribai Phule Pune University, Pune (India) 411 007*

29
30 **Abstract**

31 The rapid northward drift of the Indian plate during Deccan volcanism assumes a gradual
32 shallowing of paleomagnetic inclinations in subsequent lava flow formations. A comparison of
33 palaeomagnetic data produced during the last six decades reveals an inclination anomaly during
34 Chron C29r (66.398 - 65.688 Ma) along with brief clockwise-counter-clockwise rotations during
35 and after the main phase Deccan eruption. This interval temporally coincides with *i)* an
36 accelerated Indian ocean spreading rates, *ii)* brief incursion of an inland ‘seaway’ and *iii)* a major
37 drop in the sea level at the southern tip of the Indian Peninsula. Furthermore, the restoration of
38 tilt later during C29n agrees with the withdrawal of the inland seaway and the development of a
39 regional southward dip of the Deccan lava flow formations. Here, we produce an evolutionary
40 model to postulate the interaction of the Réunion plume with the Indian lithospheric plate with
41 coincident geological evidences demanding further exploration.

42 **Keywords:** Deccan traps; Palaeomagnetism; Indian plate; Réunion hotspot; Late Cretaceous

43
44 *: Corresponding Author e-mail: sangode@rediffmail.com

47 **Introduction**

48 Recent studies on mantle plume-lithosphere interactions indicated that spreading plume heads
49 below the lithosphere can develop significant asthenospheric flows to exert the ‘plume-push’
50 force and act as potential drivers for accelerated plate motions and/or initiation of subductions
51 (e.g., Pusok and Stegman 2020; Cande and Stegman 2011; van Hinsbergen *et al.* 2011). The
52 Deccan large igneous province (LIP) is the product of lithospheric interactions of the Réunion
53 hotspot over the northward drifting Indian plate during Late Cretaceous and early Paleogene
54 times (Courtilot *et al.*, 1986; Basu *et al.*, 1993). Geochronological records indicate a tholeiitic
55 basalt peak during 66.4-65.4 Ma, i.e., precisely within the geomagnetic Chron C29r. This peak is
56 widely referred to as the Main Deccan eruption phase (Sprain *et al.*, 2019 and references
57 therein), denoted here by the DE_M. However, the style and repercussions of the impact of the
58 Réunion mantle plume over the Indian lithospheric plate are inadequately explored (e.g. Raval
59 and Veeraswamy 2019).

60 Globally, Deccan traps represent one of the classical palaeomagnetic records with extensive
61 databases that were produced during the last six decades (e.g., Clegg *et al.*, 1955, Vandamme *et*
62 *al.*, 1991; Wensink 1973; Chenet *et al.*, 2008; 2009). We considered over 1600 statistically
63 significant mean directions obtained from all over the Deccan trap flows and dikes (Fig. 1).



64

65 **Figure 1:** Google image overlay showing the present-day extent of Deccan traps in four distinct lobes
 66 (Malwa, Mandla, Saurashtra and Central Province). The lobes (sub-provinces) lying north of the
 67 Narmada/Tapi rifts (i.e., Malwa, Mandla and Saurashtra) exhibit the records of the earliest eruptions
 68 belonging to Chron C30n as a result of northward drift of the Indian plate after its breakup from
 69 Gondwana. The pinned marks with abbreviations (expanded below) are the sites where paleomagnetic
 70 studies were undertaken. In the northern region of the central province, the majority of the normal polarity
 71 flows overlay the reverse polarity, and the rest of the occurrences with prominent reverse polarity of C29r
 72 compile the tripartite subdivision of the Deccan traps into the C30n-C29r-C29n sequence.
 73 Stratigraphically thicker (/longer) records of C29r are most widely documented in the Central province.

74 *Site Abbreviations-* Amboli (Ab) , Anjar (Aj), Akola (Ak), Ambenali (Al), Amarkantak (Am), Amravati
 75 (Av), Badargarh (Bd), Buldhana (Bu), Chincholi (Ch), Dandali (Da), Dhar (Dh), Dhule (Dl), Dindori
 76 (Dn), Dongargarh (Do), Ellora (El), Goa (Goa), Girnar (Gr), Gulbarga (Gu), Harsul (Ha), Igatpuri (Ig),
 77 Jalna (Ja), Jabalpur (Jb), Jodhpur (Jd), Jamdarwaza (Jm), Jumara (Ju), Karopani (Ka), Khairi (Ka),
 78 Kalodungar (Kd), Kelgar (Ke), Khumbharli Ghat (KG), Khandala (Kh), Kalsubai (Kl) , Khodala (Ko),
 79 Khopoli (Kp), Kanthkote (Kt), Kurduwadi (Ku), Latur (La), Linga (Li), Lonar lake (Ll), Lonavala (Lo),
 80 Matheran (Ma), Mandla Bridge (MB), Mandaleshwar (Md), Mahabaleshwar (Mh), Mandla (MI),
 81 Manikpur (Mn), Mokhada (Mo), Mohtara (Mt), Mumbai (Mu), Mundwara (Mw), Neral (Ne), Nagpur
 82 (Ng), Nipani (Ni), Panchigani (Pa), Phonda (Ph), Panhala (Pn), Pohor (Po), Pavagadh (Pv), Rewa (Re),
 83 Rajahmundry (Rj)Sadara (Sa), Sahastra Dhara (SD), Sagar (Sg), Shahapur (Sh), Singarchori(Si), Sarnu
 84 (Sr), Tapola (Ta), Trimbak (Tr), Umred (Um), Varandha Ghat (VG), Vikarabad (Vi), Wai (Wai).
 85

86 The high ferrimagnetic concentrations in the Deccan basalt mineralogy enabled classical
 87 approaches of successful demagnetization to obtain the characteristic remanence (ChRM)

88 directions referred to as primary magnetization. Here, we compiled the data from 56 widely
 89 referred publications representing the entire Deccan province, although they were largely
 90 dominated by Central Province and Chron 29r. After compilation, we classified the data into
 91 geomagnetic Chrons C30n, C29r and C29n (methods and treatment of data described below and
 92 the compiled data are available in Supplemental file). As mentioned, the Chron 29r (66.398 Ma –
 93 65.688 Ma) represents the highest number of data points in agreement with the prevailing
 94 knowledge that over 80% of the lavas erupted during this D_{EM} Chron (e.g. Renne *et al.*, 2015;
 95 Schoene *et al.*, 2015; Sprain *et al.*, 2019). The compilation observed an unambiguous inclination
 96 anomaly of more than 10° and clockwise + anticlockwise rotations of 2 to 5 degrees during C29r
 97 (see Tables 1 and 2 and the data treatment in sections below).

98 **Table 1:** An account of the mean paleomagnetic data recalculated from the database (presented
 99 in Supplemental file).

	Total data points	Mean D/I	Super-pole	Mean Inclination Data		
				C30n	C29r	C29n
Vandamme <i>et al.</i> (1991)	163	154/43 (antipode: 334/-43)	281°E 37°N	D/I ----	D/I 154/44	D/I 333/-48
This Study	1062	152/56 (antipode:332 /-56)	284°E 27°N	333/-38	157/47	341/-32
Expected Inclinations with Deccan Age-latitude relation (van Hinsbergen et al 2015)				38	35	32
Inclination Anomaly				----	12	-----

100

101 Methodology

102 The inferences and conclusions drawn in this manuscript are based on the palaeomagnetic
 103 database developed from published literature to date (from 1955 to 2020). Over 65 publications
 104 presenting palaeomagnetic approaches were published during this time, out of which over 50
 105 publications were widely and repeatedly referred independently or as cross references. The vast
 106 majority of these papers unambiguously reported directions in agreement with the N-R-N

107 sequence of the C30n-29r-29n geomagnetic polarity time scale. These data were produced
108 globally by different teams, and the analysis was performed in many different reputed
109 laboratories with varied sets of instrumental configurations and sensitivities. We elaborate here
110 on the criteria and methods adopted to compile and treat the data. We also describe the sources
111 of error and the rationale of filtering the data for mean calculations.

112 The published papers generally presented demagnetization data (using thermal or alternating
113 fields) and the estimation of characteristic remanent magnetization (ChRM) as primary
114 remanence. The routine statistical methods of spherical distribution used in paleomagnetism
115 allowed the means to be estimated at the specimen level and then at the sample level and site
116 levels. It enabled standard parameters (e.g., Alpha-95, precision parameter and maximum
117 angular deviations) to describe their scatter, facilitating global comparison. It further gives an
118 idea about the quality of data in addition to describing the normal/reverse polarities and
119 calculating the apparent and true poles. Routine statistical methods are based on the classical
120 approach of Fisher statistics (Fisher, 1967) for spherical distribution of the vector data. This
121 criterion has been used universally for rejection of the data and depiction of its quality.

122 In the majority of the papers, the reversal is unambiguously assigned to C29r, the reversal
123 followed by normal to C29r-29n, and the normal followed by reversal to 30n-29r polarity chrons.
124 The data are very well supported by field stratigraphic knowledge or chemostratigraphy. For the
125 present analysis, we complied only with the declination/inclination (D/I) directions from the
126 published literature, facilitating the site mean data points (given in the supplementary file). This
127 is because the NRM intensities are found to have large deviations due to style of presentation and
128 laboratory standards and instrumental sensitivities from individual attempts. Palaeomagnetic
129 analysis involves various protocols of demagnetization adopted by different workers and
130 instrumental sensitivities. Therefore, the standardization and comparison of NRM intensities

131 across different attempts is not feasible. However, since our inferences are founded entirely on
132 the D/I data, the NRM intensities are not considered further.

133 **Possible Sources of Error**

134 The data were retrieved and rechecked several times to check the typo errors. Below, we discuss
135 the sources of errors based on which the filtering strategy was adopted.

136 **1) Manual error:** The first and foremost source of error is generally developed during the
137 collection of oriented samples in the field. The oriented samples are collected manually (oriented
138 hand samples) or by gasoline-driven portable rock coring machines (manually handled). The
139 samples were marked carefully using either the north compass or the sun compass method. This
140 has a greater chance of introducing manual errors at various stages from marking in the field to
141 creating cylindrical specimens in the laboratory. Manual errors can also be introduced during
142 laboratory handling of specimens. For most spinner magnetometers, the samples are to be
143 handled over six directions of measurements at every stage. There is no clue to define the manual
144 error, although it may be represented in the final data as scatter that can be defined by the
145 standard palaeomagnetic data presentation procedures but with unknown contribution.

146 **2) Laboratory standards:** The palaeomagnetic data in Deccan traps are produced from various
147 laboratories that are commonly equipped with spinner magnetometers. The high NRM intensities
148 often permit complete demagnetization, even with routine spinner magnetometers with low
149 sensitivities (e.g., Minispin from Molspin UK, Sensitivity: 0.05 mA/m). The other common
150 spinner magnetometers of better sensitivities used are the DSM-Schonstedt ($\sim 10e-4$ A/m) and the
151 JR-4 to 6 series of AGICO Czech ($\sim 2.4 \times \mu\text{A/m}$). Both of these instruments thus provide better
152 confidence over a large number of palaeomagnetic data, although the quality of data carefully
153 produced from other instruments, such as Astatic magnetometers, is ascertained considering the
154 excellent repeatability and the higher intensities of the Deccan basalt samples. Furthermore, the

155 fully automated AGICO instruments prevent manual errors of sample positioning, and the
156 standardized data interface software, statistics and plotting interface allows rapid, error-free
157 processing. The cryogenic magnetometer (e.g., 2G) gives the finest sensitivity in paleomagnetic
158 analysis; however, the strong remanence in Deccan basalt does not demand such analysis unless
159 paleointensity and secular variation such as studies are aimed.

160 The detailed palaeomagnetic analysis involves demagnetization of a large array of specimens to
161 produce statistically significant data by the removal of noisy results. The two most common
162 methods of demagnetization used are thermal and alternating field demagnetizations. While
163 thermal demagnetization can introduce laboratory-induced errors during heating and cooling, af
164 demagnetization is most successful in Deccan traps due to its soft ferrimagnetic mineralogy for
165 both primary and secondary components. Individual workers have used different protocols of
166 demagnetization strategy, and the demagnetizers themselves can introduce spurious fields during
167 analysis, producing deviations rather than direct errors. Furthermore, the skills and experience of
168 individual workers during interpretation varies, which may lead to some manual bias error
169 component.

170 **a) Geomagnetic variability and transitional fields:** Some authors have indicated secular
171 variation or the non-dipole field as the source of error in paleomagnetic directions acquired by
172 few samples. However, such samples are most likely to be rejected, showing spurious directions,
173 as the palaeomagnetic directions for Deccan traps are very well known and constrained. Similar
174 is the case for the transitional polarity instances from normal to reversal and vice versa. These
175 directions are also likely rejected by the individual authors, and if they are present in the data,
176 our filtering criteria have taken care of removing such intermediate directions.

177 **b) Geotectonics:** The shield type geometry of the Deccan province in general refutes any major
178 intra-shield tectonics to affect the palaeomagnetic directions. However, the lineaments and other

179 structural features within Deccan Province, if contemporary, can be inferred for tectonically
180 induced errors. Few authors have reported such tectonic relations, but they are mainly related to
181 vertical movement rather than internal rotations and deformation and do not express any major
182 anomaly in paleomagnetic data. These references justifying the tectonic component are avoided
183 in our database approach. Chron C29r is the main focus of this study, and the majority of the
184 palaeomagnetic data for this chron belong to the main/central Deccan province, which does not
185 show such intra-shield tectonics at large to affect the internal rotations and tilt. If such
186 incoherence is present, it should be reflected by deviation of D/I directions internally, for which
187 we have applied the filtering criteria discussed below.

188 ***Data Reduction (rejection) and Filtering***

189 The Deccan traps represent one of the richest databases for a short geological interval of less
190 than 5 Ma, marked by the distinct polarity zone of N-R-N of the Late Cretaceous/Paleogene. The
191 ample data produced globally from different laboratories are within close agreement, and a
192 simple filtering and reduction of data based on routine spherical distribution statistics is feasible.
193 A previous compilation made by Vandamme *et al.* (1991) resulted in defining the Deccan Super
194 pole based on contemporarily available data. With the updated database up to 2020, we
195 recalculated the Deccan Super pole, which is in close agreement with Vandamme et al 1991 (see
196 Table 1). The deviation of values seen in this table is simply due to enrichment by the new data
197 during the latter 30 years since the publication of Vandamme et al 1991. Therefore, considering
198 these Super pole directions as central tendencies, we defined the limits/windows for filtering out
199 the data, apart from rejecting the data with large scatter defined by the precision parameter (k)
200 and alpha-95 of Fisher statistics.

201
202 ***Table 2: Considering the means for whole data in 5th column of Table 1 as the central tendency***
203 ***of the updated database, we further applied filters to remove the noise in data due to the possible***

204 errors described above. The data for C30n, C29r and C29n are filtered individually in a
 205 declination window of +/- 36 (10% of 360) and inclination window of +/-18 (10% of 180).
 206

	Chron 30n		C29r		C29n	
	D	I	D	I	D	I
Central Tendency	333	-38	157	47	341	-32
Window	297-366	20-56	121-193	29-65	305-377	14-50
Means after Filter	338	-38.7	153.3 (333.3 antipode)	47.4	334.8	-35.1
Stats	A95: 2.5; k = 21.37, N:153		A95: 1.1, k = 36.05, N: 451		A95: 4.3, k:21.61, N:54	
Anomaly with Vandamme <i>et al.</i> 1991	+4 (clockwise)	-5 (shallow)	-0.7 (anticlock)	+5 (deeper)	+0.8 (clockwise)	-8 (shallow)
Anomaly with expected inclination at Réunion latitudes		0.7		12.4		3

207
 208 **Table 3:** The Inclination Anomaly for C29r with respect to inclinations from various approaches
 209 described in text (inclination for C29r is taken as 47°).
 210

Reference	Inclination in degrees	Anomaly Amount in Degree
w.r.t. Expected latitudes by $\tan I = 2 \tan \lambda$ ($\lambda = 20.5$ to 21.5)	~36 to 38	11 to 9
w.r.t. C30n	38 (table 1)	9
w.r.t. C29n	32 (table 1)	15
w.r.t. C30n Filtered Mean	47.4-38.7	8.7
w.r.t. C29n Filtered Mean	47.4-35.1	12.3
w.r.t. latitudinal mean	47.4-37	10.4
Average for expression in the text.....		10.78

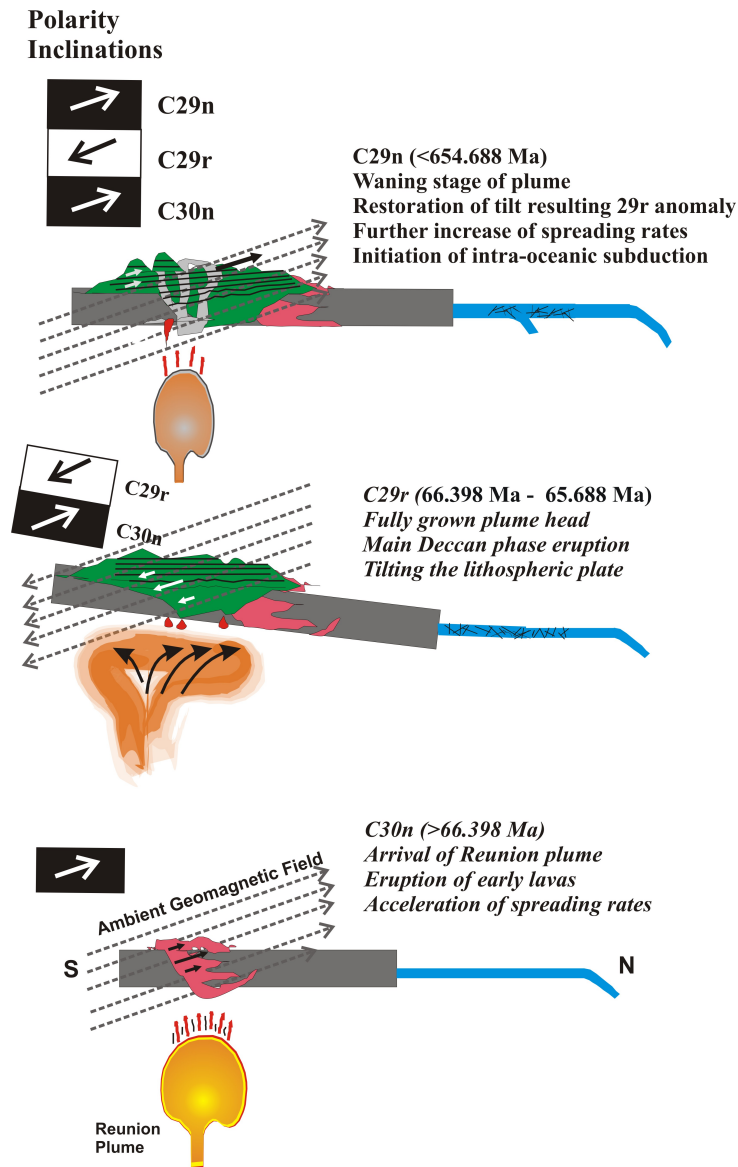
211
 212
 213
 214
 215 **Table 4:** Rotational anomaly (+: clockwise, -: anticlockwise).
 216

	Filtered Mean	Wrt Reference North	Inferred Indian plate rotation
29n	334.8	-25.2	2 degree anticlockwise wrt 29r
29r	333.3	-26.7	5 degree clockwise wrt 30n
30n	338	-22	
During 80 to 60 Ma		-12	

217
218
219
220
221
222
223
224
225
226
227
228
229
230

The Inclination Anomaly and Rotation

The observed mean inclination for C29r is significantly higher than the anticipated paleolatitude derivative of 35°, and an average value of 10.78 can be assigned from various approaches expressed in Table 3. This ‘+10°’ inclination anomaly observed during C29r is simply a mathematical expression of a significant northerly dip of the Indian plate. It is much oversighted in the context of equatorward drift of the Indian plate, which anticipates either inclination shallowing or, at most, inclination values intermediate to C30n and C29n. Moreover, no record of such large magnitude changes during the Late Cretaceous geodynamo does exist (Coe *et al.*, 2000; Pechersky *et al.*, 2010; Velasco-Villareal *et al.*, 2011) and therefore also refutes the geodynamo effect. In contrast, coincident geological evidence from the Indian subcontinent endorses the anomaly by possible effects of plate tilting (Fig. 2 and the evidence produced below).



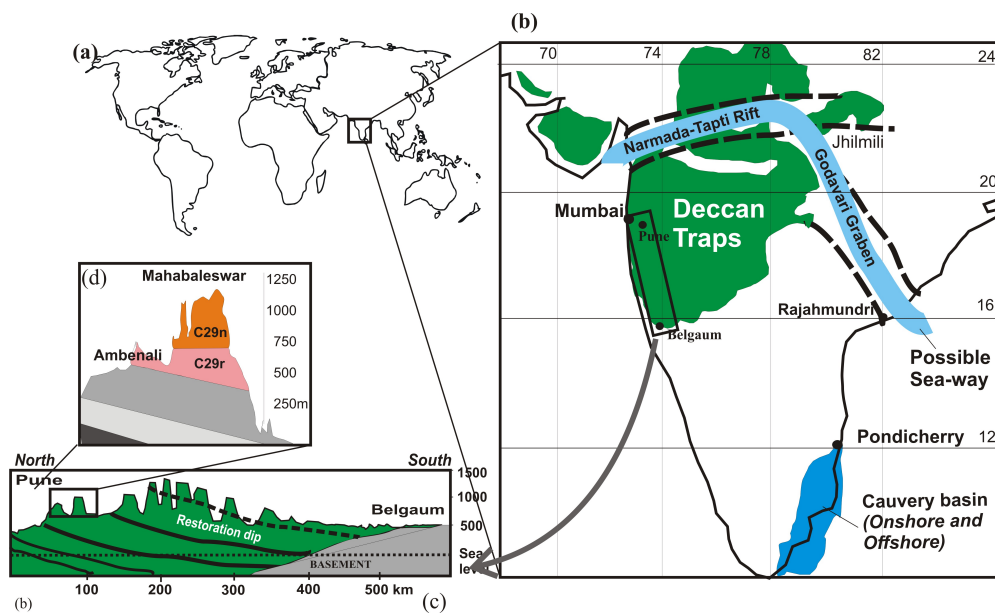
231

232 **Figure 2.** Evolutionary staged model to depict the mechanism of geodynamic interaction of
 233 Indian plate with the Réunion plume/hotspot imparting the inclination anomaly. During C30n,
 234 the subcontinent approached the impinging mantle plume, as documented by the alkaline
 235 magmatism in the northern part of the Deccan province. The interaction of the Indian plate with
 236 a fully developed plume head further during C29r resulted in a north/northeast tilt to record the
 237 ambient reverse field. As the plate moved farther from the waning plume, the tilt was restored,
 238 and the reverse inclination steepened, producing the inclination anomaly of C29r (detailed in
 239 text).

240

241 Very high inclinations ($D/I=140/60^\circ$) during C29r are reported from the Deccan trap rocks of the
 242 Cauvery region in southern India (Mishra *et al.* 1989), and although the data are inadequate, they
 243 suggest a southern extent. The pre-Deccan Late Cretaceous strata from the Cauvery Basin on the

244 southern Peninsula record a shallower inclination (338/-38, N=80) (Venkateswarulu 2020),
 245 substantiating the existence of the Deccan anomaly. The inclinations for C29n and C30n agree
 246 well with the anticipated paleolatitudes (Table 3), which indicates that the tilt was absent in C30n
 247 and restored during C29r as the Indian plate drifted away from the Réunion plume head (e.g., see
 248 Fig. 2). The regional southward dip for the Deccan lava flows (Fig. 3) is widely documented (Jay
 249 and Widdowson 2008; Shoene *et al.* 2015) and verify our proposed model based on
 250 palaeomagnetic inclination (Figure 3).



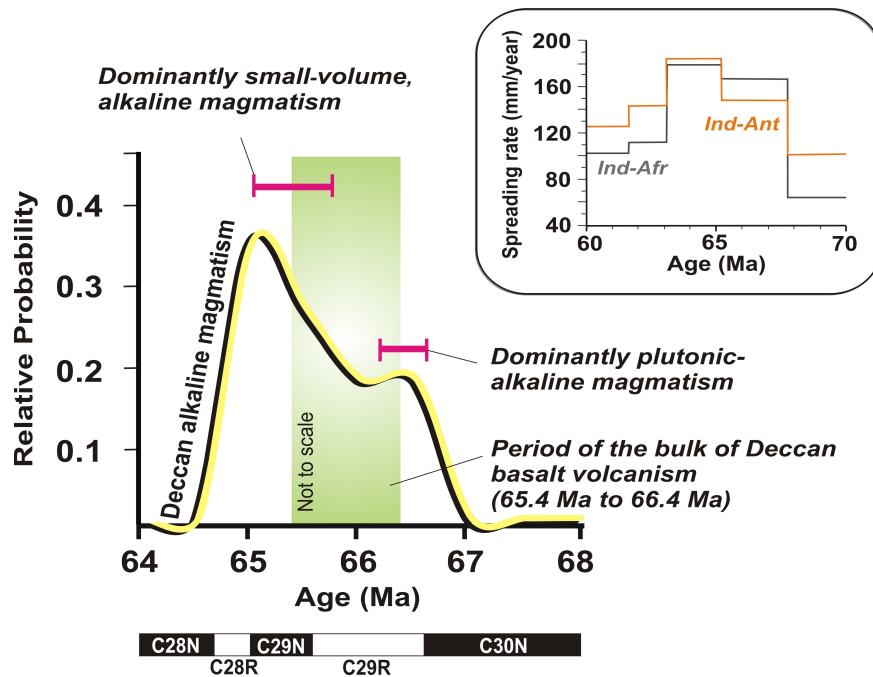
251
 252 **Figure 3.** (a) World map showing the location of Deccan Province, (b) India showing the present
 253 extent of Deccan trap province and the possible seaway as reported from biostratigraphic records
 254 and the location of Cauvery Basin documenting a significant drop in sea level during the Late
 255 Cretaceous. The widely reported Pune to Belgaum (N-S) profile (c) depicts a regional dip,
 256 explained here as a result of tilt restoration (discussed in text). Inset (d) shows the dip
 257 discordance between C29r (Ambenali Formation) and C29n (Mahabaleswar Formation) marked
 258 in Schoene *et al.* (2021), supporting tilt and restoration.
 259

260 Considering the tilt and rotation estimates from the palaeomagnetic database (Tables 1 to 4), we
 261 further confirm our model by supporting geological evidence accounted below.

262
 263
 264

265 *Magmatic records of plume head arrival and plate tilt*

266 There is a close temporal and spatial linkage between voluminous LIPs, their tholeiitic and
267 alkaline magmatism and mantle plumes (e.g., Bryan and Ernst 2007). The LIPs are generally
268 characterized by short-lived (<1-5 Ma) igneous pulses responsible for large volume (>75%)
269 magma outpours. Alkaline rocks associated with LIPs are typically formed due to low degrees of
270 partial melting of mantle owing to minor thermal effects from an impinging or receding mantle
271 plume (e.g., Gibson *et al.* 2006). The impact of the Réunion plume over the Indian plate is in
272 close agreement with this convention through the observed episodes of tholeiitic and alkaline
273 magmatism. The initial impact of the Réunion plume head started ~0.2 million years before the
274 DE_M and produced nepheline syenites and alkali gabbros during these early Deccan eruptions
275 (Fig. 3), corresponding to terminal C30n/early C29r. Recent high-precision geochronological
276 data (Renne *et al.*, 2015; Sprain *et al.*, 2019) indicated outpouring of bulk Deccan tholeiites
277 between 65.4 and 66.4 Ma within C29r. This rapid extrusion requires higher amounts of partial
278 melting under a considerably elevated geothermal gradient during a fully developed plume head,
279 which precisely coincides with the duration of C29r (Cande and Kent, 1995). Small-volume
280 volatile-rich magmatism of lamprophyres and carbonatites between 65.8-65.2 Ma (Fig. 3), which
281 was mostly emplaced towards the terminal part of the DE_M, typically intruded the Deccan lavas.
282 This terminal phase is an artifact of small-fraction melting caused by thermal weakening during
283 the waning stage of the Réunion plume. The occurrence of DE_M precisely within C29r therefore
284 elucidates the short span (<1 million years) of geodynamic interaction of the plume head with the
285 Indian plate. This rapid impact of the plume head below the western margin of the Indian plate
286 therefore appears to have resulted in tilt and rotation, as recorded by the paleomagnetic data.



287

288 **Figure 4.** Relative probability of alkaline and small-volume, volatile rich magmatism spatially
 289 and temporally related to the Deccan LIP based on high-precision $^{40}\text{Ar}/^{39}\text{Ar}$ and U-Pb
 290 determinations (n=12) (adopted from Dongre, *et al.* 2021). The period of bulk Deccan basalt
 291 volcanism is also shown in green (from Sprain *et al.*, 2019). Inset: Spreading rates between
 292 India-Antarctica and India-Africa ridges (After Cande and Stegman, 2011).
 293

294 *Accelerated convergence at the end of C29r*

295 The spreading rates in the Indian Ocean reached a maximum between ~66 and 63 Ma during
 296 C29n (Cande and Stegman, 2011; compiled and redrawn in Fig. 4). The initial anomalously high
 297 rates of drift of the Indian plate from less than 100 mm/y to ~160 mm/y during 68 to ~66 Ma are
 298 explained by the arrival of the plume head (Eagles and Hoang, 2014). Therefore, the later
 299 increase in spreading (up to 180 mm/y after ~66 Ma) during the waning and withdrawal stages of
 300 the plume/plume head needs to be explained. We postulate this later increase in convergence
 301 rates as a result of *i*) the termination of plume-induced rotational and tilt components that
 302 resolved into northward drifting kinematics, in addition to *ii*) the establishment of double
 303 subduction.

304

305 *Acceleration of the intra-oceanic subduction*

306 Mantle plumes have been considered drivers of regional subduction initiation (Gerya *et al.* 2015;
307 Pusok and Stegman 2020; van Hinsbergen *et al.* 2021, Rodriguez *et al.* 2021). Multiple
308 subductions are evident for the India-Asia convergence; however, the final subduction during
309 ~66 Ma to 65 Ma is little explored in the context of Deccan volcanism and the Réunion plume
310 push force. We infer that the quick geodynamic response of the Indian plate over the Réunion
311 plume head during DE_M marked by the tilt and counter rotations during C29r might have exerted
312 significant changes in pre-existing plate kinematics at the India-Asia subduction interface.
313 Possible resultant deformation due to plate tilt and rotation added to the previously accelerated
314 rate of convergence may have significant repercussions on the initial stage of intraoceanic
315 subduction (Fig. 2). The combination of quick clockwise and anticlockwise rotations along with
316 tilt and drift appears to have superimposed over the pre-existing kinematics for the Indian plate
317 demanding detailed kinematic modelling in this context.

318 *Opening of the ‘Sea-way’ within the plate*

319 Based on paleontological finds, a short-lived ‘seaway’ associated with Deccan traps has been
320 reported precisely at the end of C29r (e.g. Keller *et al.* 2009, 2012). This inland ‘sea-way’
321 formation (/marine influence) along pre-existing rift valleys (i.e. Narmada and Godavari Rifts,
322 shown in Fig. 3) is evident by the stressed marine fauna. The brief north/northeast tilting of the
323 Indian plate therefore offers a possibility to explain the formation of the brief inland ‘sea-way’.
324 Biostratigraphically well-documented localities ~800-1000 km inland of the Narmada and
325 Godavari rifts contain brief and stressed planktic foraminiferal assemblages within terrestrial
326 palustrine to freshwater facies (Keller *et al.* 2009, 2012). The absence of benthic species among
327 these localities (Keller *et al.* 2012) indicates only a brief marine incursion that can be explained
328 by a major tectonic event such as the lithospheric tilt reported here. The paleosols developed

329 over this zone designate upland conditions and further support the restoration of tilt during C29n,
 330 as depicted in Figure 2. The late Maastrichtian rocks of the Cauvery Basin at the southern tip of
 331 Peninsular India represent fluvial formations overlain by marine to estuarine formations and
 332 record a vertical sea level fall of 80 m (Nagendra and Reddy 2017; Raju et al 1994). Thus,
 333 upliftment of the southern peninsular tip of the Indian plate is documented and marked by a rapid
 334 sea level fall during the deposition of the Kallamedu Formation (Late Maastrichtian) in the
 335 Cauvery Basin. The contemporaneous upliftment of the southern end of the Indian plate along
 336 with downward tilt in northern and northeastern Deccan provinces indicate plume head-induced
 337 tilting.
 338 Finally, although more geological evidence with precise dating is required, the present
 339 perceptions (Fig. 2-4 and Table 4) strongly support the geodynamic developments over the
 340 Indian plate precisely during C29r and the main Deccan eruption.

341
 342 **Table 5:** A summary of sequence of events presented in the paper.
 343

Time	Stage	Event
30n	Plume early stage	Indian plate encountered the Réunion hotspot
Late 30n to Early 29r	Emerging plume-lithosphere interaction	Indian plate encountered the plume over western continental margin and rotated clockwise possibly by thermal expansion (and uplift) of the lithosphere in the plume region. Eruption of early lavas and alkaline rocks. Acceleration of spreading rates.
Early to Late 29r	Fully developed plume head	Maximum exposure of the plate to plume, eruption of bulk of Deccan basalts, possible upliftment of the southern Peninsular part of the Indian plate along with tilting in the N/NE part of the plate, biostratigraphic evidences of 80m drop in sea level in south and opening of the seaway in N/NE periphery of Deccan. Quick clockwise-anticlockwise rotations along with northward tilt appears to have developed a weak zone possibly leading to the latest subduction in the India-Eurasia zone.
29n		Waning stage of the plume, restoration of tilt, regional south dip of Deccan, closure of seaway, onset of secondary subduction

344

345 The present findings have larger implications for understanding the plate-wide impact of plume-
346 lithospheric interactions. This may further lead to detailed investigations on the response of
347 concurrent geological consequences related to Réunion plume-lithospheric interactions over the
348 Indian plate during Deccan trap volcanism.

349

350 **Acknowledgements**

351 We indirectly acknowledge all the authors who produced and published the palaeomagnetic data
352 over the years cited in this paper. SJS, AND AB acknowledge Ministry of Earth Sciences for the
353 grant MoES/P.O.(Seismo)/1(353)/2018. All the authors acknowledge Head, Department of
354 Geology SPPU, for support during the pandemic.
355

356 There are no conflict of interests.

357

358 **References**

- 359 Basu, A.R., Renne, P.R., Dasgupta, D.K., Teichmann, F., Poreda, R.J., 1993, Early and Late Alkali
360 Igneous Pulses and a High-3He Plume Origin for the Deccan Flood Basalts. *Science* 261, p. 902-
361 906.
- 362 Bryan, S. and Ernst, R., 2008, Revised Definition of Large Igneous Province (LIP), *Earth Science*
363 *Reviews*. doi: 10.1016/j.earscirev.2007.08.00.
- 364 Cande, S.C. and Kent, D.V., 1995, Revised calibration of the geomagnetic polarity timescale for the
365 Late Cretaceous and Cenozoic. *Journal of Geophysical Research*, 100, p. 6093-6095.
- 366 Cande, S.C. and Stegman, D.R. 2011, Indian and African plate motions driven by the push force of the
367 Réunion plume head. *Nature* 475, p. 47–52.
- 368 Chenet, A.L., Courtillot, V., Fluteau, F., Gérard, M., Quidelleur, X., Khadri, S.F.R., Subbarao, K.V.,
369 Thordarson, T., 2009, Determination of rapid Deccan eruptions across the Cretaceous–Tertiary
370 boundary using paleomagnetic secular variation: 2. Constraints from analysis of eight new sections
371 and synthesis for a 3500-m-thick composite section: *Journal of Geophysical Research* 114/38. doi:
372 10.1029/2008JB005644.
- 373 Chenet, A.L., Fluteau, F., Courtillot, V., Gerard, M., Subbarao, K.V., 2008, Determination of rapid
374 eruption across the Cretaceous–Tertiary boundary using paleomagnetic secular variation: Results
375 from a 1200 m thick section in the Mahabaleshwar escarpment. *Journal of Geophysical Research*
376 113 (B4), B04101.
- 377 Clegg, J.A., Deutsch, E.R., Griffiths, D.H., 1956, Rock magnetism in India, *Philos. Mag.*, 1, p. 419-
378 431.
- 379 Coe, R.S., Hongre, L., Glatzmaier, G., 2000, An examination of simulated geomagnetic reversals from a
380 palaeomagnetic perspective *Phil. Trans. R. Soc. A.*, 358, p. 1141–1170
381 [http://doi.org/10.1098/rsta.2000.0578\(2000\)](http://doi.org/10.1098/rsta.2000.0578(2000))
- 382 Courtillot, V., Besse, J., Vandamme, D., Montigny, R., Jaeger, Cappetta, H., 1986, Deccan flood
383 basalts at the Cretaceous/Tertiary boundary? *Earth and Planetary Science Letters* 80, P. 361-374.
- 384 Dongre, A., Dhote, P.S., Zamarkar, P., Sangode, S.J., Belyanin, G., Meshram, D.C., Patil, S.K.,
385 Karmakar, A., Jain, L., 2021, Short-lived alkaline magmatism related to Réunion plume in the
386 Deccan large igneous province: inferences from petrology, ⁴⁰Ar/³⁹Ar geochronology and

387 paleomagnetism of lamprophyre from the Sarnu-Dandali alkaline igneous complex. Geological
388 Society London Special Publications 513. <https://doi.org/10.1144/SP513-2021-34>

389 Eagles, G. and Hoang, H., 2014. Cretaceous to present kinematics on the Indian, African and Seychelles
390 plates. *Geophysical Journal International* 196, p. 1-14.

391 Gerya, T.V., Stern, R.J., Baes, M., Sobolev, S.V., Whattam, S.A., 2015, Plate tectonics on the Earth
392 triggered by plume-induced subduction initiation. *Nature*, 527, p. 221-225, doi:10.1038/nature15752.

393 Gibson, S.A., Thompson, R.N., Day, J.A. 2006, Timescales and mechanisms of plume- lithosphere
394 interactions: ⁴⁰Ar/³⁹Ar geochronology and geochemistry of alkaline igneous rocks from the Parana-
395 Etendeka large igneous province. *Earth and Planetary Science Letters* 251, p., 1-17.

396 Jay, A.E. and Widdowson, M., 2008, Stratigraphy, structure and volcanology of the south-east Deccan
397 continental flood basalt province: implications for eruptive extent and volumes. *Journal of the*
398 *Geological Society London* 165, p. 177-188.

399 Keller, G., Adatte, T., Bajpai, S., Mohabey, D.M., Widdowson, M., Khosla, A., Sharma, R., Khosla,
400 S.C., Gertsch, B., Fleitmann, D., Sahni, A., 2009, K-T transition in Deccan Traps and intertrappean
401 beds in central India mark major marine seaway across India. *Earth and Planetary Science Letters*
402 282, p. 10–23. doi:10.1016/j.epsl.2009.02.016.

403 Keller, G., Adatte, T., Bhowmick, P.K., Upadhyay, H., Dave, A., Reddy, A.N., Jaiprakash, B.C. 2012,
404 Nature and timing of extinctions in Cretaceous-Tertiary planktic foraminifera preserved in Deccan
405 intertrappean sediments of the Krishna-Godavari Basin, India. *Earth and Planetary Science Letters*
406 341–344, p. 211–221. doi:10.1016/j.epsl.2012.06.021.

407 Mishra, D.C., Gupta, S.B., Venkatarayudu, M., 1989, Godavari rift and its extension towards the east
408 coast of India. *Earth and Planetary Science Letters*, 94, p. 344-352.

409 Nagendra, R. and Reddy, A.N., 2017, Major geologic events of the Cauvery Basin, India and their
410 correlation with global signatures: A review. *Journal of Palaeogeography*, 6(1), p. 69-83.

411 Pechersky, D.M., Lyubushin, A.A., Sharonova, Z.V., 2010, On the synchronism in the events within the
412 core and on the surface of the earth: The changes in the organic world and in the polarity of the
413 geomagnetic field in the phanerozoic. *Physics of the Solid Earth* 46, p. 613-623.

414 Pusok, A.E., and Stegman, D.R., 2020, The convergence history of India-Eurasia records multiple
415 subduction dynamics processes. *Science Advances* 6, eaaz8681.

416 Raju, D.S.N, Jaiprakash, B.C., Ravindran, C.N., Kalyanasunder, R., Ramesh, P. 1994, The magnitude of
417 hiatus and sea level changes across the K T boundary in Cauvery and Krishna Godavari Basin. *Jour.*
418 *Geol. Soc. India*, 44, p. 301-315.

419 Raval, U., and Veeraswamy, K., 2019, Some apparent space-time mismatches (puzzles) over the Indian
420 subcontinent and channeling. *Journal of the geological society of India*. 93, p. 25-32.

421 Renne, P.R., Sprain, C.J., Richards, M.A., Self, S., Vanderkluyesen, L., Pande, K., 2015, State shift in
422 deccan volcanism at the cretaceous-Paleogene boundary, possibly induced by impact. *Science*
423 350(6256), p. 76-78.

424 Rodriguez, M., Arnould, M., Coltice, N., Soret, M., Hoang, E., 2021, Long-term evolution of a plume-1
425 induced subduction in the Neotethys realm. *Earth and Planetary Science Letters* 561, 116798.
426 <https://doi.org/10.1016/j.epsl.2021.116798>

427 Schoene, B., Eddy, M.P., Keller, C.B. and Samperton, K.M., 2021, An evaluation of Deccan Traps
428 eruption rates using geochronologic data. *Geochronology*, 3, p. 181–198

429 Schoene, B., Samperton, K.M, Eddy, M.P., Keller, G., Adatte, T., Bowring, S., Khadri, S.F.R., Gertsch,
430 B., 2015, U-Pb geochronology of the Deccan traps and relation to the end cretaceous mass
431 extinction. *Science* 347, p. 182-184.

432 Sprain, J., Renne, P.R., Vanderkluyesen, L., Pande, K., Self, S., Mittal, T. 2019, The eruptive tempo of
433 Deccan volcanism in relation to the Cretaceous- Paleogene boundary. *Science* 363, p., 866-870.

434 van Hinsbergen, D. J. J., Lennart V. de Groot, Sebastiaan J. van Schaik, Wim Spakman, Peter K. Bijl,
435 Appy Sluijs, Cor G. Langereis, and Henk Brinkhuis, 2015, A Paleolatitude Calculator for
436 Paleoclimate Studies (model version 2.1), PLOS ONE

437 van Hinsbergen, D.J.J., Steinberger, B., Doubrovine, P.V., Gassmüller, R., 2011, Acceleration and
438 deceleration of India-Asia convergence since the Cretaceous: Roles of mantle plumes and
439 continental collision. *Journal of Geophysical Research* 116. doi:10.1029/2010jb008051.
440 Vandamme, D., Courtillot, V., Besse, J., Montigny, R. 1991, Palaeomagnetism and age determinations
441 of the Deccan Traps (India); results of a Nagpur– Bombay traverse and review of earlier work.
442 *Reviews of Geophysics* 29, p. 159–190.
443 Velasco-Villareal, M., Urrutia-Fucugauchi, J., Rebolledo-Vieyra, M., Perez-Cruz, L., 2011,
444 Paleomagnetism of impact breccias from the Chicxulub crater - Implications for ejecta emplacement
445 and hydrothermal processes. *Physics of the Earth and Planetary Interiors* 186, p. 154–171.
446 Venkateshwarlu, M., 2020, New paleomagnetic pole and magnetostratigraphy of the Cauvery Basin
447 sediments, southern India. *J Earth Syst Sci* 129, 222. <https://doi.org/10.1007/s12040-020-01476-z>.
448 Wensink, H., 1973, Newer paleomagnetic results of the Deccan traps, India. *Tectonophysics* 17, p. 41-
449 59.